PAPER REFERENCE: *ICF10010130R*

FATIGUE STRENGTH AND FRACTURE MECHANISM OF SILICON NITRIDES STUDIED BY AE WAVEFORM SIMULATION

A. Yonezu, T. Ogawa and M. Takemoto

Department of Mechanical Engineering, Aoyama Gakuin University,
6-16-1 Chitosedai, Setagaya, Tokyo 157-8572, Japan

ABSTRACT

In order to evaluate statistical characteristics of static and cyclic fatigue strength of a toughened silicon nitride, both the quasi-static loading test and ΔP-increasing-type cyclic loading test were conducted with simultaneous acoustic emission (AE) monitoring. Waveform matching of the zero-th order symmetric mode Lamb AE waves were attempted to study the fracture dynamics. Crack volumes estimated by the AE waveform simulation was compared with those computed by three dimensional FEM. Fracture mechanisms of toughened silicon nitride under static and cyclic fatigue were discussed in detail.

KEYWORDS

Silicon nitride, Static fatigue, Cyclic fatigue, Weibull distribution, Fatigue damage, Acoustic emission, Waveform matching, Fracture Mechanism

INTRODUCTION

It has been well recognized that sintered silicon nitrides, Si_3N_4, exhibit both static and cyclic fatigue behaviour [1]. Since the fatigue strength generally shows a large scatter, it should be evaluated by a statistical expression of *S-N* curve, namely *P-S-N* curve. However, the statistical evaluation requires a time-consuming and expensive work. One of the authors proposed a simple method to evaluate the fatigue strength statically under a mechanical condition where driving force for fracture is gradually increased [2]. This technique enabled us to study the statistic characteristics of fatigue strength and contribution of fatigue damage with respect to the testing conditions.

Mechanism of the fatigue damage of toughened silicon nitride is be caused by initiation and growth of small cracks [3]. However, the conventional optical observation is extremely difficult because crack initiation site is hardly predicted. Source location method of AE signals enables the estimation of crack initiation position. Further, the inverse processing or waveform simulation can study the fracture dynamics such as crack nucleation time, ΔT_r, and crack volume, ΔV [4], and supply us with information of damage mechanism. In the present study, both static and cyclic fatigue strength of toughened Si_3N_4 was studied utilizing new-type loading procedure and AE waveform simulation to monitor the behaviour of small cracks in the ceramic.

MATERIAL AND EXPERIMENTAL PROCEDURES

The material tested is a hot-isostatically sintered silicon nitride, Si_3N_4, developed by NGK Spark Plug Co. The density is measured as 3310 kg/m^3. Fracture toughness (SEPB) and four point bending strength are 9.8 $\mathrm{MPa}\sqrt{\mathrm{m}}$ and 729 MPa, respectively. Rectangular bar specimen (3x4x40 mm) was subjected to four point bending with inner span of 10 mm and outer spans of 30 mm, at room temperature in air using hydraulic testing machine with load capacity of 10 kN.

Figure 1(a) illustrates loading history of ΔP-increasing-type cyclic test. Stress ratio, R, of the cyclic loading is controlled as 0.1 and the cyclic loading frequency, f, is 20 Hz. Testing parameters of the ΔP-increasing test are the initial value, $\sigma_{max,i}$, of maximum stress, σ_{max}, and increasing rate of σ_{max}, $d\sigma_{max}/dN$(=2.8x10^{-4} MPa/cycle). Provided that the value of $\sigma_{max,i}$ is sufficiently lower than σ_{max} at failure, $\sigma_{max,f}$, all the specimens tested are broken by cyclic loading, and the $\sigma_{max,f}$ value is evaluated for the individual specimens, as schematically illustrated in Fig. 2, where the effect of $\sigma_{max,i}$ is investigated. When the $\sigma_{max,f}$ values are analysed by Weibull distribution, fatigue strength can be evaluated statistically. Similarly, static fatigue strength can be evaluated by P-increasing test as illustrated in Fig. 1(b).

Figure 3 shows AE monitoring system used. Two resonant-type AE sensors (Ch.1 and 2, PAC, PICO, center frequency of 0.58MHz) with a diameter of 4mm are mounted on the upper surface of the specimen opposite to the outer pins. Sensor outputs are amplified by a 40dB preamplifier and digitised by an A/D converter at a sampling interval of 50 ns with 1024 points at 10 bits. As the sensors monitor continuous noise with low frequency due to cyclic contacts of the specimen to two pins, trigger signal for AE events is prepared by using a new circuit. It has two functions of adding two sensor's output and of filtering out the lower frequency components (-20 dB at 100kHz and -2 dB at 1 MHz).

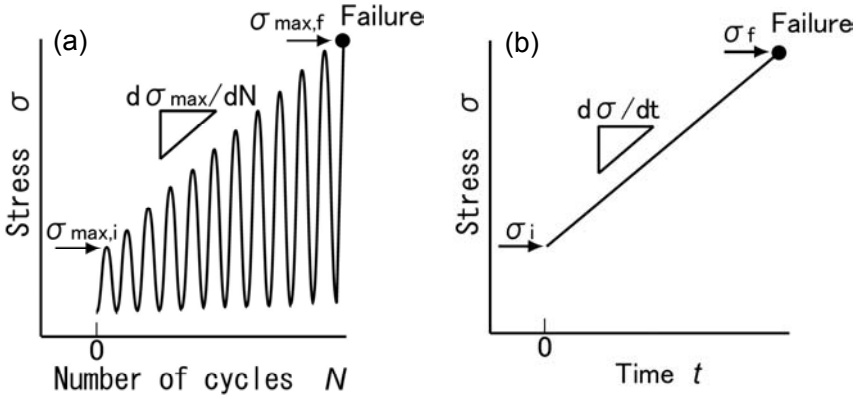

Figure1: Loading sequences of the (a)ΔP-increasing test (cyclic fatigue) and (b)P-increasing test (static fatigue).

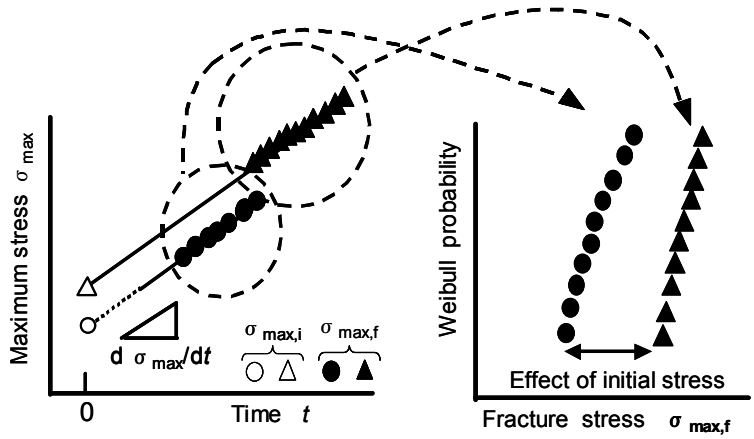

Figure.2: Schematic illustration of the ΔP-increasing tests and statistical analysis evaluating the effect of $\sigma_{max,i}$ on $\sigma_{max,f}$.

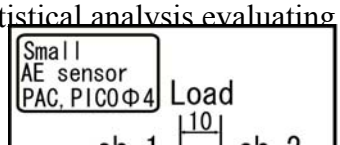

RESULTS AND DISCUSSION

Figure 4 presents the Weibull plots of σ_f and $\sigma_{max,f}$ for quasi-static and cyclic loading conditions, respectively. Also presented is a flexural strength measured under monotonic loading condition at the crosshead speed of 0.5 mm/min [5]. Despite the loading rate is 10^4 times lower, the σ_f values well agree with the flexural strength. This strongly suggests that there is no dependence of time, namely no static fatigue strength degradation. However, cyclic fatigue degradation clearly appeared in this material. ΔP-increasing tests with different $\sigma_{max,i}$ enabled us to evaluate the cyclic loading condition under which fatigue damage nucleated. The result suggested that $\sigma_{max,i}$ influenced the $\sigma_{max,f}$ values for statistically weak specimens and thus fatigue damage developed at lower stress levels.

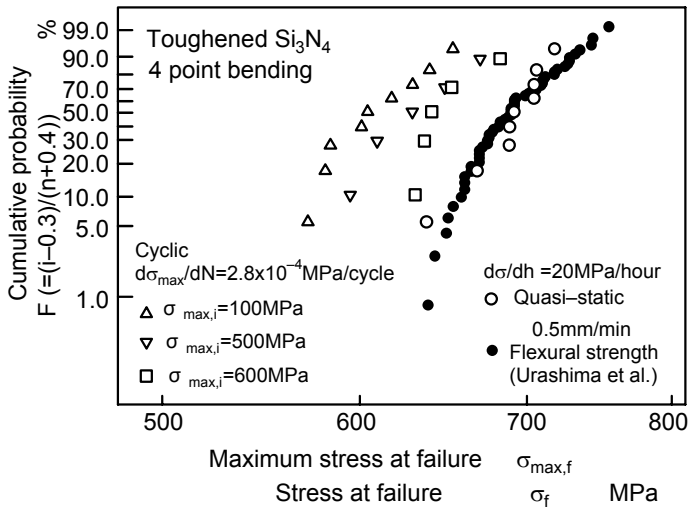

Figure 4: Weibull plots of σ_f and $\sigma_{max,f}$ in toughened Si_3N_4.

Detail signal analysis demonstrated that the AE events detected contain both symmetric (S_0) and anti-symmetric (A_0) mode Lamb wave of zero-th order. First arrival time and waveform of the S_0-Lamb mode were utilized for source location and fracture dynamics study. Source location results are shown in Fig. 5 for quasi-static (a) and cyclic (b) loadings. The location was estimated by using arrival time difference of So-mode and its group velocity for the specimens with average strength for these loading conditions. The abscissa is an axial location of specimens, where the origin is a left edge of specimen. Inner span and final fracture location are indicated by broken lines and solid line, respectively. The vertical axis represents stress values at fracture. The results revealed that a few AE signals were detected at stresses just below the final fracture value near the fracture locations.

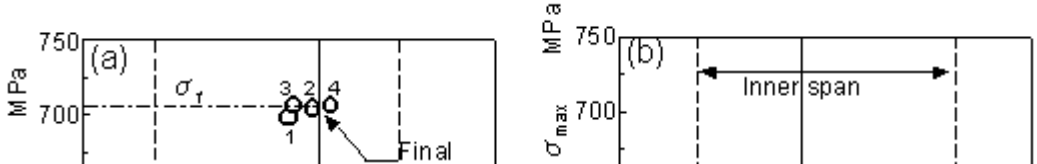

The fracture dynamics were studied by the S_0-packet waveform matching. Detail of this method can be found elsewhere [6]. The overall transfer function, including the sensor, medium and AE monitoring system, was determined by the method shown in Fig. 6. Lamb-wave AE signals were exited by a compression-mode PZT element, glued to a specimen and stainless steel block by epoxy, and were monitored by PICO sensor. Here, the out-of-plane displacement of PZT element was monitored by a laser interferometer and converted to time transient of crack volume. The overall transfer function for the Lamb-wave due to Mode-I crack opening was obtained by the time-domain Gauss-Zeidel deconvolution of the detected waves by the PICO sensor. Crack opening was represented by a sinusoidal rump function with rise time, ΔT_r, and crack volume, ΔV. They were determined by matching the simulated waveform of the S_0-packet to the detected one.

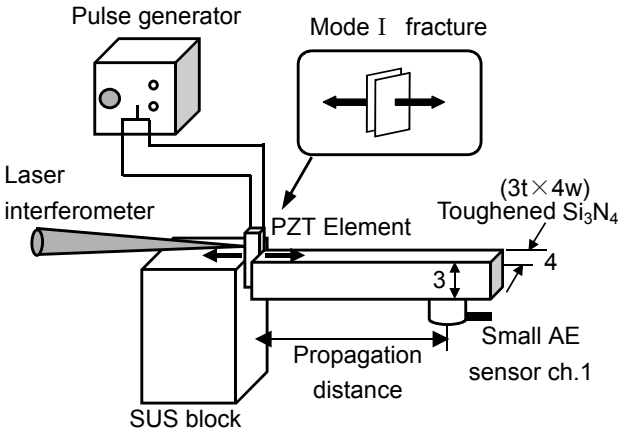

Figure 6: Experimental setup to determine the overall transfer function.

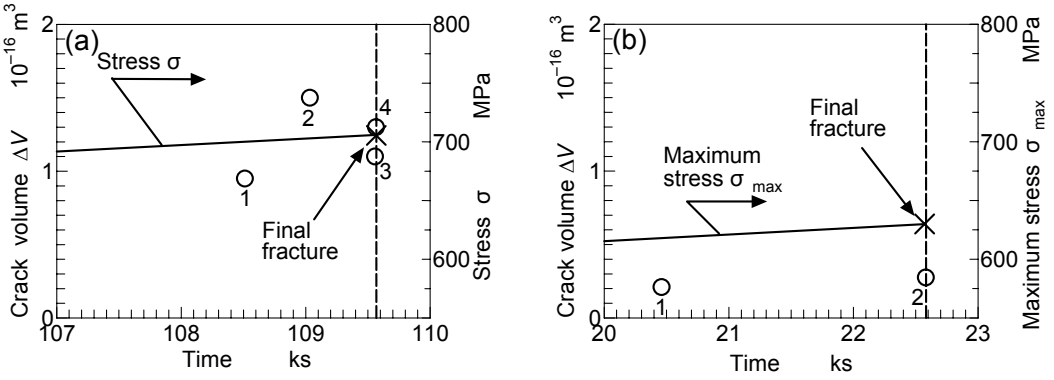

Figure 7: AE source volumes as a function of applied stresses for the quasi-static(a) and the cyclic(b) loading.

Figure 7 shows ΔV estimated for quasi-static (a) and cyclic (b) loadings with stress values as a function of testing time. The numbers in the figure indicate event count. The crack volume produced during the cyclic loading was estimated to be six times smaller than that produced during static loading at lower stress level.

Source rise time, ΔT_r, was estimated as 0.11 μs, which was the lower limit of our AE system. First AE signals for both loading conditions were monitored at more than 1 ks before the final fracture. These results suggest that cyclic loading enhances nucleation of small cracks.

The initial crack was observed at large-grown columnar β-Si_3N_4 under both loadings, as shown in Fig. 8. Sizes of the β-Si_3N_4 were about 90μm long and 20μm wide. Similar microstructure was observed on fracture surfaces of all the specimens tested. Next computed the crack opening displacement by three-dimensional finite element method (FEM) using MARC (K7-2). The model is illustrated in Fig. 9. Crack initiation location shown in Fig.8 (a) and (b) are modelled as in Fig. 9 (b) and (c), respectively. Total numbers of elements are 7168 (b) and 5488 (c). Displacements of axial direction on the tensile surface were constrained except the rectangular area surrounded by broken line. Axial displacements of the rectangular area are referred to a half of crack opening displacement and are used to determine the crack volume, ΔV, under the fracture load. The values of ΔV under quasi-static (b) and cyclic (c) loadings were calculated as 1.18×10^{-16} and 2.95×10^{-16} m^3, respectively. For the quasi-static loading, the crack volumes estimated by the AE waveform matching well agreed with that produced at columnar β-Si_3N_4, while those for the cyclic loading were ten times smaller than ΔV estimated by FEM. The cyclic loading appears to produce discontinuous small cracks along the columnar β-Si_3N_4.

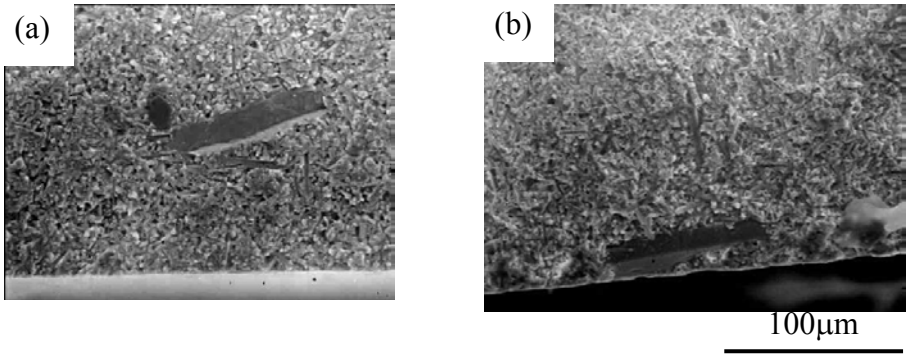

Figure 8: SEM photographs of fracture surfaces under the quasi-static loading(a) and the cyclic loading(b). AE analysis shown in Figure 7 and 11 was performed for these specimens.

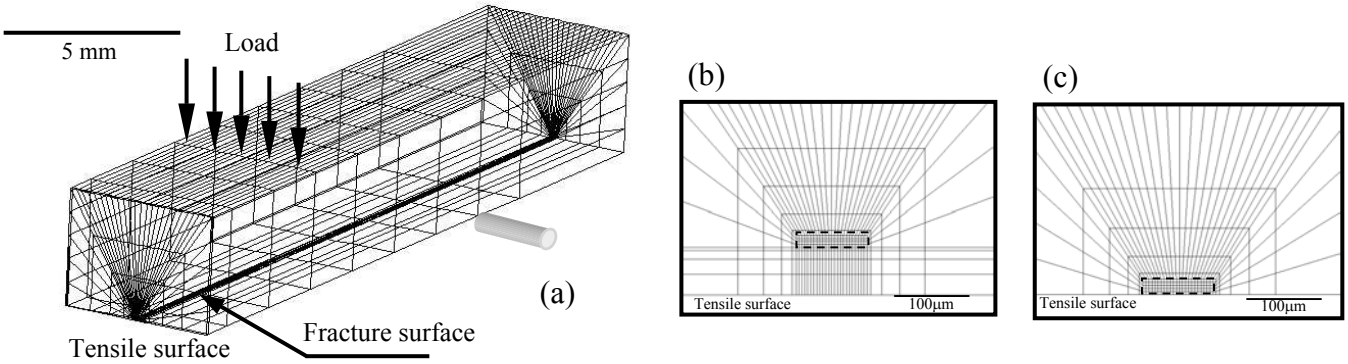

Figure 9: Three-dimensional finite element model (a) and initial cracks modeled for the quasi-static(b) and the cyclic(c) loadings.

Fatigue mechanism of the toughened Si_3N_4 is summarized as follows. Under the quasi- static loading, cracks with the size of large-grown columnar β-Si_3N_4 were initiated very quickly at the load level just below the fracture stress. Under the cyclic loading, crack initiation occurred under lower stress level with smaller initial size than under quasi-static loading. The small crack grew and led fast fracture. Cyclic fatigue damage can be regarded as the above small crack initiation, which developed under more than 100 MPa below the fracture stress level for statistically weak specimens. Early stage of the fatigue damage could not be detected by our AE monitoring system.

CONCLUSIONS

Both static and cyclic fatigue strength of toughened Si_3N_4 was investigated using new loading method and

AE waveform matching method. Results are summarized below:

1. No static fatigue strength degradation was found for this ceramic, while cyclic fatigue degradation appeared.
2. ΔP-increasing tests with different initial value of maximum stress, $\sigma_{max,i}$, enabled us to evaluate the cyclic loading condition under which fatigue damage nucleated. The result suggested that $\sigma_{max,i}$ influenced the maximum stress at failure, $\sigma_{max,f}$, for statistically weak specimens and thus fatigue damage developed at lower stress levels.
3. Crack volume produced during the cyclic loading was estimated by Lamb AE waveform matching method and found to be six times smaller than that produced during static loading.
4. Initial crack was observed at large-grown columnar β-Si_3N_4 under both loadings. For the quasi-static loading, the crack volumes estimated by the AE waveform matching method well agreed with that produced at columnar β-Si_3N_4, while those for the cyclic loading were ten times smaller than ΔV estimated by FEM.
5. Fatigue mechanism of the toughened Si_3N_4 is discussed based on the strength distribution and AE results.

ACKNOWLEDGEMENTS

Authors are grateful to Dr. Urashima, NGK Spark Plug Company, for supplying the toughened silicon nitride specimens.

REFERENCES

1. T. Yamada, T. Hoshide and H. Furuya, J. Soc. Mat. Sci., Japan, 33(364), 28-33(1983) [in Japanese].
2. T. Ogawa, Proc. The 13th European Conference on Fracture, Elsevier Science CD, 186C1.PDF, p.8 (2000).
3. O. Ritchie and H. Dauskardt, J. Ceramics Society Japan 99(10), 1047-1062(1991).
4. M. Takemoto, O. Tamura and H. Suzuki, Progress in Acoustic Emission IX, Ⅲ, 81-88(1998).
5. K. Urashima, Y. Tajima, M. Enoki and T. Kishi, Proc.11th Forum on Basic Science of High Temperature Ceramics, 66-70(1992).
6. T. Sato, M. Takemoto and K. Ono, Jpn Appl. Phys., 39, 3193-3200(1999).